

Stabilization of High-Valent Molecular Cobalt Sites through Oxidized Phosphorus in Reduced Graphene Oxide for Enhanced Oxygen Evolution Catalysis

Jiahui Yang⁺, Guoliang Dai⁺, Wenjuan Song, Poe Ei Phyu Win, Jiong Wang,* and Xin Wang*

Abstract: Heterogeneous molecular cobalt (Co) sites represent one type of classical catalytic sites for electrochemical oxygen evolution reaction (OER) in alkaline solutions. There are dynamic equilibriums between Co^{2+} , Co^{3+} and Co^{4+} states coupling with OH^-/H^+ interaction before and during the OER event. Since the emergence of Co^{2+} sites is detrimental to the OER cycle, the stabilization of high-valent Co sites to shift away from the equilibrium becomes critical and is proposed as a new strategy to enhance OER. Herein, phosphorus (P) atoms were doped into reduced graphene oxide to link molecular Co^{2+} acetylacetone toward synthesizing a novel heterogeneous molecular catalyst. By increasing the oxidation states of P heteroatoms, the linked Co sites were spontaneously oxidized from 2+ to 3+ states in a KOH solution through OH^- ions coupling at an open circuit condition. With excluding the Co^{2+} sites, the as-derived Co sites with 3+ initial states exhibited intrinsically high OER activity, validating the effectiveness of the strategy of stabilizing high valence Co sites.

Introduction

Water electrolysis represents a promising approach for sustainable conversion of renewable energy into chemical fuels with high energy density.^[1] The anodic oxygen evolution reaction (OER) consists of multiple proton-coupled electron transfer (PCET) steps, which exhibits inherent high energy barriers, leading to high overpotentials. While noble metal oxides of IrO_2 and RuO_2 are considered as the benchmark catalysts in acidic medium,^[2] their practical application is limited by relatively high cost and low structural stability. Therefore, it is essential to develop highly efficient alkaline OER catalysts made of non-precious elements which can replace noble metal based catalysts. Co-based compounds (e.g., oxides, hydroxides and sulfides, etc) with octahedral Co active sites have exhibited promising OER activity.^[3] In general, Co sites undergo sequential redox processes (Co^{2+} , Co^{3+} to Co^{4+} states), known as PCET reactions, to generate high-valent Co sites (e.g., Co-oxo species) for overcoming the OER barriers.^[4] In an OER cycle, the Co site stays at 3+ and 4+ states. In the meantime, there are dynamic equilibriums between Co^{2+} , Co^{3+} and Co^{4+} states since their redox processes are commonly quasi-reversible; and the desorption of oxygen species, as the final elemental step of OER, is a reduction process. These would result in the emergence of Co^{2+} sites in the OER process, which would block the reaction cycle.^[4a,5] In addition, the OER rate scales with overpotentials and is typically dictated by $\text{Co}^{2+/3+}$ redox potentials. Such a dictation establishes an intrinsic limit for enhancing OER, and is commonly observed in various molecular electrocatalytic processes involving the redox of catalytic sites.^[6] Thus, to stabilize the high-valent Co^{3+} or Co^{4+} sites (or increase their concentration) with deactivating the $\text{Co}^{2+/3+}$ redox is critical toward achieving highly efficient OER, while it remains a challenge together with identifying the relevant valence-structure correlations.^[4d]

Heterogeneous molecular catalysts (HMCs) recently have been developed to exhibit great potential in the OER research field.^[7] Such catalysts are achieved through surface immobilization of metal complexes onto solid conductive support, which combines both the advantages of traditional heterogeneous and homogeneous catalysis, including affording high turnover frequencies (TOFs), being durable in aqueous solutions and serving as an appropriate platform for mechanism investigations at the molecular level.^[8] Carbonaceous materials are widely used as solid supports of

[*] J. Yang,⁺ W. Song, P. E. P. Win, Prof. J. Wang
 Innovation Center for Chemical Science, College of Chemistry,
 Chemical Engineering and Materials Science
 Soochow University
 Suzhou 215006, Jiangsu, P. R. China
 E-mail: wangjiong@suda.edu.cn
 J. Yang,⁺ P. E. P. Win, Prof. J. Wang
 Jiangsu Key Laboratory of Advanced Negative Carbon Technologies
 Soochow University
 Suzhou, 215123, Jiangsu, P.R. China
 Prof. G. Dai⁺
 School of Chemistry and Life Sciences
 Suzhou University of Science and Technology
 Suzhou 215009, Jiangsu, P. R. China
 X. Wang
 Department of Chemistry
 City University of Hong Kong
 Hong Kong, 999077, P. R. China
 E-mail: wang.xin@cityu.edu.hk
 [+] These authors contributed equally: J. Yang and G. Dai

molecular catalysts due to their high specific surface area, electrical conductivity and stability. In particular, by doping P heteroatoms, it can result in structural deformation of carbon frameworks due to the relatively large atomic diameter of P atoms, which protrude from carbon plane to function as linking sites. Since the P atom ($\chi=2.19$) has lower electronegativity than the C atom ($\chi=2.55$), this would result in positively charged P atoms in carbon frameworks.^[9] Besides, P atoms can be oxidized into P oxide (PO_x) species under harsh synthesis conditions, resulting in less steric effects from the carbon frameworks toward linking molecular catalysts, and the linking sites can exhibit stronger electron withdrawing ability.^[10] Such structural properties could be advantageous for surface immobilization and stabilization of high-valent Co sites, thus achieving highly efficient OER catalysis.

Based on the above consideration, in this work, various P doped reduced graphene oxide samples was synthesized by a common hydrothermal method, and the incorporated PO_x species were applied for linking simple Co^{2+} acetylacetone ($\text{Co}(\text{acac})_2$) to generate a series of Co based HMCs. The oxidation levels of P heteroatoms were tuned. It was found that $\text{PO}(\text{OH})_2$ based linkage promoted the Co sites to become electron deficient. Taking advantage of the PECT nature, such linked Co sites spontaneously oxidized from 2+ to 3+ states in a KOH solution through OH^- ions coupling at an open circuit condition. The Co sites were thus stabilized at 3+ states prior to OER, which exhibited intrinsically improved OER activity comparing to one with 2+ initial states. A high turnover frequency of 0.87 s^{-1} for Co sites was achieved at an overpotential of 0.35 V.

Results and Discussion

A phosphorus-doped reduced graphene oxide (P_1G) was firstly synthesized using graphene oxide as the precursor and phenylphosphine (P_1) as the dopant, which was realized under a hydrothermal condition. $\text{Co}(\text{acac})_2$ was anchored onto P_1G in *N,N*-dimethylformamide (DMF) as previously reported.^[4b] The resultant sample is denoted as $\text{P}_1\text{G}-\text{Co}^{2+}$ (all the details have been provided in Supporting Information, [SI]). As measured by inductively coupled plasma optical emission spectroscopy (ICP-OES, Table S1), the Co content of $\text{P}_1\text{G}-\text{Co}^{2+}$ is $4.5 \times 10^{-7} \text{ mol mg}_{\text{P}_1\text{G}}^{-1}$. Scanning and transmission electronic microscopic (SEM/TEM) images of $\text{P}_1\text{G}-\text{Co}^{2+}$ present typical graphene characters without observing possible Co oxides/hydroxides (Figure 1A and S1). Focusing on the carbon layers, energy-dispersive X-ray (EDX) spectra suggest there is homogeneous distribution of Co species (Figure 1B and Figure S2). In an aberration corrected high-angle annular dark-field scanning transmission electron microscopic image (AC HAADF-STEM, Figure 1C), substantial discrete bright spots (size $<0.5 \text{ nm}$) emerge, indicating that the Co species of $\text{P}_1\text{G}-\text{Co}^{2+}$ are at the molecular scale. Such structural characters are reflected by X-ray diffraction (XRD) patterns and Raman spectra (Figure S3 and S4). Ultraviolet-visible (UV/Vis) spectra show the $\pi-\pi^*$ transition band of P_1G at 268 nm and metal-

to-ligands charge transition (MLCT) band of $\text{Co}(\text{acac})_2$ at 277 nm. The absorbance band of $\text{P}_1\text{G}-\text{Co}^{2+}$ shifted to 273 nm (Figure 1D). Besides, in electron paramagnetic resonance (EPR, Figure 1E) analysis, $\text{P}_1\text{G}-\text{Co}^{2+}$ shows a singlet peak similar as $\text{Co}(\text{acac})_2$. The *g* value shifted from 2.11 to 2.04 for the arising from the spin-orbit coupling in the Co centers. It suggests that the Co sites of $\text{P}_1\text{G}-\text{Co}^{2+}$ stay at 2+ oxidation state, while there is less electron filling of Co sites ongoing from $\text{Co}(\text{acac})_2$ to $\text{P}_1\text{G}-\text{Co}^{2+}$.^[11] According to X-ray photoelectron spectroscopic (XPS, Figure 1F and Figure S5) surveys, upon the immobilization of $\text{Co}(\text{acac})_2$ onto P_1G , the Co 2p core levels positively shifted by about 0.58 eV. The P 2p core levels negatively shifted by about 0.97 eV. Thus, it is speculated that there is efficient electron communication between Co and P sites in $\text{P}_1\text{G}-\text{Co}^{2+}$, which well supports the EPR data.

Figure 1G shows the Co K-edge X-ray absorption near-edge structure (XANES) data of $\text{P}_1\text{G}-\text{Co}^{2+}$, Co foil, CoO and Co_3O_4 . The rising edges of Co K-edge absorption curve of $\text{P}_1\text{G}-\text{Co}^{2+}$ is similar to those of CoO and $\text{Co}(\text{acac})_2$, indicating that the Co sites of $\text{P}_1\text{G}-\text{Co}^{2+}$ have 2+ oxidation state. Besides, upon interacting with P_1G , the Co oxidation state slightly increased, which is consistent with the XPS data. The coordination spheres of Co sites were investigated by Fourier-/Wavelet-transformed extended X-ray absorption fine structure (FT/WT EXAFS). It verified that the Co sites of $\text{P}_1\text{G}-\text{Co}^{2+}$ maintained molecular dispersion (Figure 1H). According to the quantitative least-squares EXAFS fitting analysis (Figure 1I, S6–S8 and Table S2), the first sphere of $\text{P}_1\text{G}-\text{Co}^{2+}$ is contributed by two types of Co–O scattering path. One Co–O path has four coordination number that can be ascribed to the acac^- ligand (Co–O1), and the other Co–O path has one coordination number that can be assigned to the linking of P_1G support (Co–O2).

The OER performance of as-synthesized $\text{P}_1\text{G}-\text{Co}^{2+}$ was evaluated on a rotation disk electrode (RDE) by linear scanning voltammograms (LSVs) in 1 M KOH. During the test, the RDE was maintained at 1600 rpm to remove generated bubbles (all potentials were referred to reversible hydrogen electrode, RHE, if not specified). The potentials of LSVs were compensated by 95% *iR* loss. To tune the oxidation states of P heteroatoms in reduced graphene oxide and investigate their impacts on the Co sites based OER electrocatalysis, phenylphosphinic acid (P_2) and phenylphosphonic acid (P_3) were respectively used as phosphorus dopants to synthesize other types of P-doped reduced graphene oxide (i.e., P_2G and P_3G , Table S3) following the same procedures as the synthesis of P_1G . The GO was also treated by the hydrothermal condition in the absence of phosphorus dopants, and it derived the reduced graphene oxide simply carrying oxygen heteroatoms (OG) for comparison. Upon immobilizing $\text{Co}(\text{acac})_2$ onto P_2G , P_3G and OG, the control samples were derived and denoted as $\text{P}_2\text{G}-\text{Co}^{2+}$, $\text{P}_3\text{G}-\text{Co}^{2+}$ and $\text{OG}-\text{Co}^{2+}$, respectively (Figure S9–S12). As shown in Figure 2A, the OER overpotential of $\text{P}_1\text{G}-\text{Co}^{2+}$ is as low as 370 mV (defined as the potential corresponds to current density of 10 mA cm^{-2} and subtracts the equilibrium potential). This is clearly superior to that of $\text{OG}-\text{Co}^{2+}$ (440 mV), as well as those of $\text{P}_2\text{G}-\text{Co}^{2+}$ (400 mV) and $\text{P}_3\text{G}-\text{Co}^{2+}$

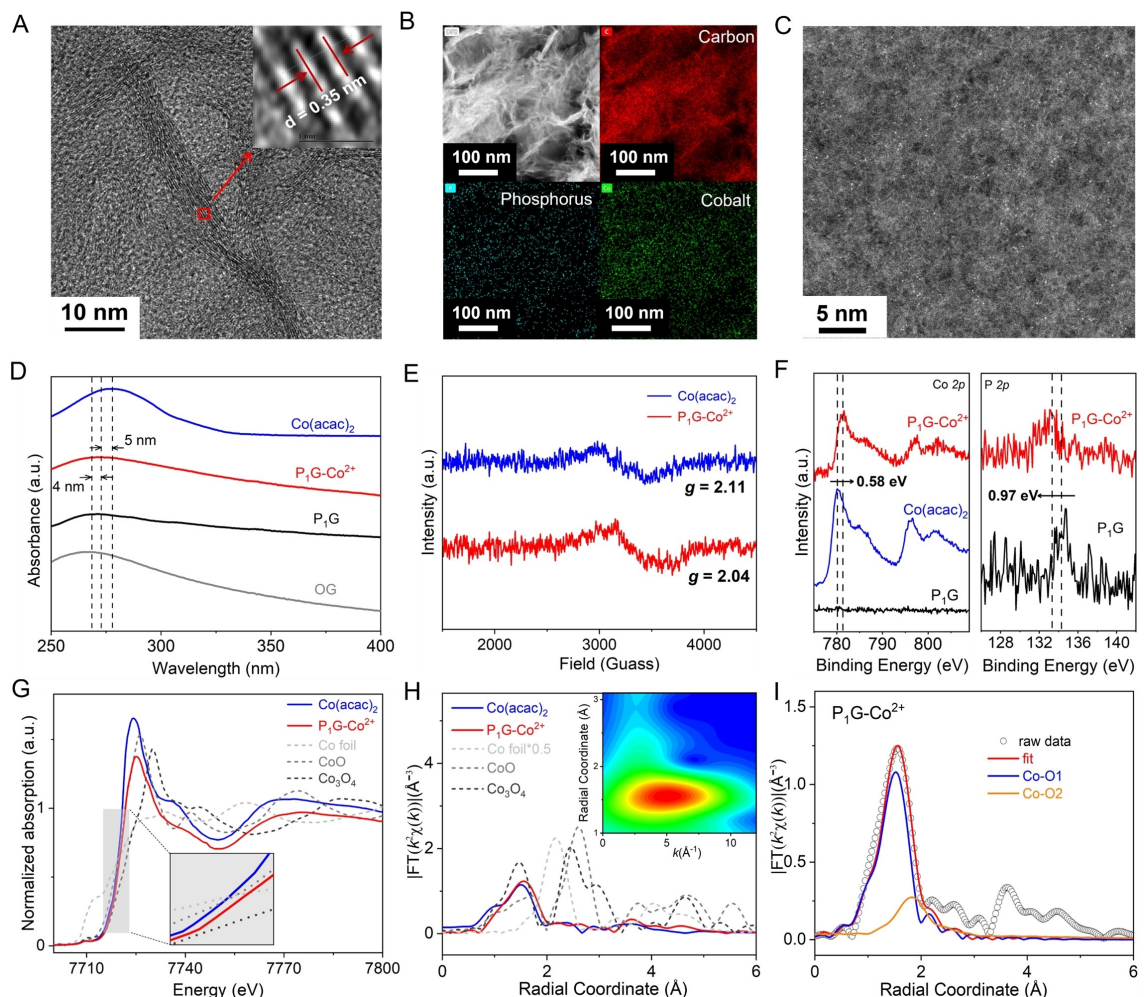


Figure 1. Structural characterizations of molecular Co sites. (A) A bright field TEM images of $P_1G\text{-Co}^{2+}$. Inset shows the fast Fourier transform inverse pattern for the selected region. (B) A dark field TEM image of $P_1G\text{-Co}^{2+}$ with corresponding elemental mapping images of C, P and Co elements by EDX analysis. (C) An AC HAADF-STEM image of $P_1G\text{-Co}^{2+}$. (D) UV/Vis spectra of P_1G , $P_1G\text{-Co}^{2+}$, OG and $\text{Co}(\text{acac})_2$. (E) EPR spectra of $P_1G\text{-Co}^{2+}$ and $\text{Co}(\text{acac})_2$ collected at room temperature. (F) XPS surveys of Co 2p core levels of P_1G , $\text{Co}(\text{acac})_2$ and $P_1G\text{-Co}^{2+}$ (left panel) and P 2p core levels of P_1G and $P_1G\text{-Co}^{2+}$ (right panel). (G) Co K-edge XANES data of $\text{Co}(\text{acac})_2$ and $P_1G\text{-Co}^{2+}$, and the data of Co foil, CoO and Co_3O_4 are included for comparison. Inset shows the rising edges. (H) Corresponding FT-EXAFS data in R-space. Inset shows the WT-EXAFS data of $P_1G\text{-Co}^{2+}$. (I) EXAFS R-space fitting of $P_1G\text{-Co}^{2+}$.

(420 mV). In order to verify the Co based catalytic sites, the OER performance of Co-free P_1G , P_2G and P_3G were tested, which are all insignificant (Figure S13). Thus, the turnover frequencies (TOFs) of each catalyst were calculated by normalizing the OER currents with overall and surface amounts of Co sites, respectively (i.e., TOF_{sum} and TOF_{surf}). Being consistent with the LSVs, $P_1G\text{-Co}^{2+}$ afforded the highest TOF_{sum} and TOF_{surf} (e.g., 0.49 s^{-1} and 0.87 s^{-1} at an overpotential of 0.35 V) among the various catalysts (Figure 2B and 2C), following a clear activity trend of $P_1G\text{-Co}^{2+} > P_2G\text{-Co}^{2+} > P_3G\text{-Co}^{2+} > OG\text{-Co}^{2+}$. This suggests that the Co sites of $P_1G\text{-Co}^{2+}$ are intrinsically active, and the TOFs of $P_1G\text{-Co}^{2+}$ are superior to many Co based catalysts reported recently (Table S4). Moreover, in a long-term measurement, the current density of $P_1G\text{-Co}^{2+}$ kept durable at 1.65 V without apparent decline (Figure 2D). We did not observe the possible formation of Co oxides or hydroxides,

and the possible corrosion of P_1G support, as gained from XRD, Raman and XPS surveys (Figure S14). $P_1G\text{-Co}^{2+}$ was reacted with ethylenediaminetetraacetic acid (EDTA) aqueous solution after the long-term measurement.^[4b,12] Due to the strong chelation of EDTA, the ligands of Co^{2+} sites in $P_1G\text{-Co}^{2+}$ were replaced to form EDTA–Co complexes. The UV/Vis spectra showed the characteristic absorbance of EDTA–Co complex at 533 nm (Figure S15).^[13] In contrast, after mixing EDTA with standard Co_3O_4 solids under the same condition, the resultant EDTA solution did not present any EDTA–Co signals. This also verified that $P_1G\text{-Co}^{2+}$ kept molecular states after the long-term measurement.

The electrochemical properties of $P_1G\text{-Co}^{2+}$ were studied in KOH solutions with pH ranging from 12.3 to 14 for the Pourbaix analysis. It showed the redox peaks at 0.4 – 0.65 V (vs. Hg/HgO) assigned to the typical $\text{Co}^{3+/4+}$ couple

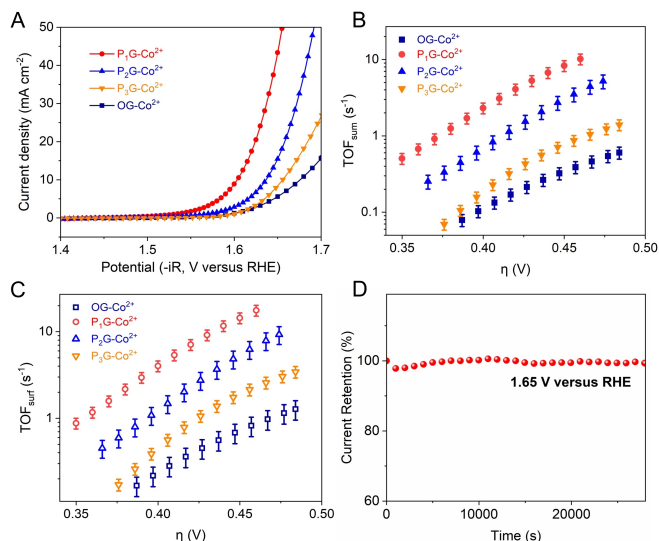


Figure 2. OER performance of molecular Co sites. (A) LSVs of OG-Co²⁺, P₁G-Co²⁺, P₂G-Co²⁺ and P₃G-Co²⁺ conducted at 10 mV s⁻¹ scan rate, 1 M KOH, 1600 rpm. The potentials are compensated by 95 % *iR* loss. TOF_{sum} (B) and TOF_{surf} (C) of Co sites for OER obtained based on the overall and surface amounts of Co sites, respectively. (D) A chronoamperometric curve of P₁G-Co²⁺ conducted at 1.65 V, 1 M KOH.

(Figure S16).^[14] For the anodic potentials, the pH dependence is linearly fitted to be 0.123 V pH⁻¹, which suggests that Co³⁺-to-Co⁴⁺ oxidation events couple with OH⁻ ions (i.e., decouple with H⁺ ions) by a stoichiometry of 1:2. Strikingly, the pH dependence of cathodic potentials has a linear slope of 0.062 V pH⁻¹, showing that Co⁴⁺-to-Co³⁺ reduction events decouple with OH⁻ ions (i.e., couple with H⁺ ions) by a stoichiometry of 1:1 (Figure 3A).

Thus, it is speculated that one of the coupled OH⁻ ions in the Co³⁺-to-Co⁴⁺ oxidation is irreversible, which should have been further involved into the OER cycle. A galvanostatic titration was conducted at 0.2 mA cm⁻². The potentials were linearly scaled to solution pH values by a linear slope of 0.077 V pH⁻¹ (Figure 3B and Figure S17). It is known that TOFs are proportional to the dynamic current density and exponentially depend on overpotentials. TOFs are also related to the activities of reactants (i.e., a_{OH⁻}), which is measured by pH (i.e., pH = -log[a_{H⁺}]). The pH dependence of OER is analyzed based on the following equation (1).

$$\left(\frac{\partial E}{\partial pH} \right)_j = \left(\frac{\partial E}{\partial \log(j)} \right)_{pH} \left(\frac{\partial \log(j)}{\partial pH} \right)_E \quad (1)$$

As the Tafel slope of P₁G-Co²⁺ is fitted to be 0.078 V dec⁻¹ (Figure S18), the log of current density is derived to be linearly scaled with pH value by a slope of 1.0. To verify this, we measured the pH dependence of OER current density (Figure 3C, Figure S16 and S19). By either the galvanostatic or voltammetric methods, a linear slope was obtained (i.e., 0.99/0.93). This is consistent with the calculated data, indicating the first order dependence of OER on the concentrations of OH⁻ ions. In addition, an in situ attenuated total reflection Fourier transform infrared

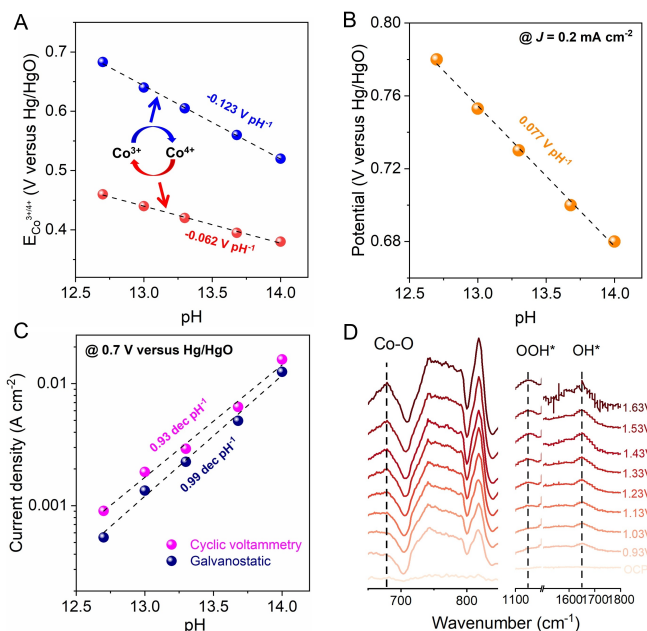


Figure 3. Coupling of OH⁻ ions with molecular Co sites for OER. (A) Pourbaix diagram of Co^{3+/4+} redox in various KOH solutions varying from pH 12.7 to 14. (B) pH dependence of OER potentials on P₁G-Co²⁺ in various KOH solutions. The current density was constant of 0.2 mA cm⁻². (C) pH dependence of OER current densities on P₁G-Co²⁺ in various KOH solutions. (D) In situ ATR-FTIR of OER on P₁G-Co²⁺.

(ATR-FTIR) spectral analysis was performed ranging from open circuit potential (OCP) to 1.63 V on P₁G-Co²⁺ (Figure 3D). No obvious peaks were found at OCP. Upon applying potentials, one peak appeared at 1645 cm⁻¹ for the stretching and bending vibrations of adsorbed OH⁻ species.^[15] Meanwhile, a signal simultaneously emerged at 678 cm⁻¹ for the generated Co-O bonds due to the OH⁻ species interacting with Co sites, verifying the Pourbaix data of Co^{3+/4+} couple.^[16] From 1.33 V onwards, another peak emerged at 1148 cm⁻¹ as an indication of the formation of OOH* species.^[17] This is considered as the key step toward forming dioxygen, which demonstrated the OER process on P₁G-Co²⁺. Accordingly, combining with the previous literatures,^[4b,c] we proposed a general OER pathway on P₁G-Co²⁺ as, L-Co³⁺(OH⁻) → L-Co⁴⁺(O²⁻) → L-Co⁴⁺(O²⁻)(OH⁻) → L-Co³⁺(OOH) → L-Co³⁺(O₂) (L denotes the residual ligands on the Co sites).

Commonly for Co species, their Co^{2+/3+} redox occurs in the range of 1.0–1.1 V prior to the redox of Co^{3+/4+} couple. However, P₁G/P₂G-Co²⁺ exhibited insignificant Co^{2+/3+} redox, while it is clear in the case of P₃G-Co²⁺ (Figure 4A). The Co^{2+/3+} redox charges were integrated to calculate the electroactive amounts of Co sites on each catalyst, and were normalized by the amounts of Co sites on the electrode surfaces obtained from ICP-OES. This derived the redox response of Co^{2+/3+} couple, which is inversely related to the TOF_{surf} of Co sites (Figure 4B, Table S5). Note that according to the ICP measurements, the surface amounts of Co sites in those catalysts are very close, which should not cause

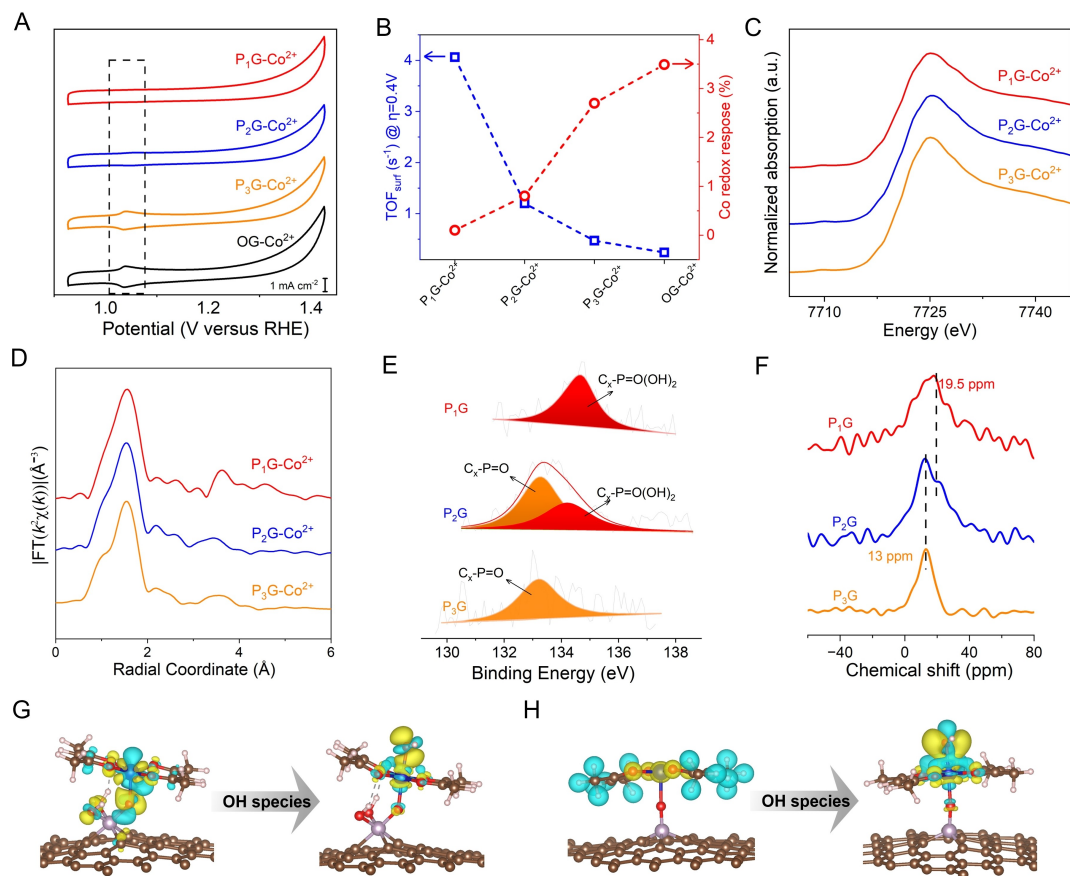


Figure 4. Tuning the oxidation states of molecular Co sites. (A) CVs of OG-Co²⁺, P₁G-Co²⁺, P₂G-Co²⁺, P₃G-Co²⁺, 50 mV s⁻¹ scan rate, 1 M KOH. (B) TOF_{surf} of Co sites for OER at $\eta = 0.4$ V, and their correlation with the redox response of Co sites as determined from integrating the redox peaks of Co^{2+/3+} couple. (C) Co K-edge XANES data of P₁G-Co²⁺, P₂G-Co²⁺, and P₃G-Co²⁺. (D) Corresponding FT-EXAFS data in R-space. XPS surveys of P 2p core electron levels (E) and ³¹P NMR (F) of P₁G, P₂G and P₃G. (G) The calculated charge density difference for P₁G-Co²⁺ before and after interacting with OH species. (H) The calculated charge density difference for P₃G-Co²⁺ before and after interacting with OH species. Yellow and blue regions represent electron accumulation and depletion, respectively. OER started from the chemisorption of H₂O, followed by generating OH*, O[·], OOH* and O₂ species.

the tuned redox responses of Co sites. According to the XANES data (Figure 4C), P₁G/P₂G/P₃G-Co²⁺ all have the 2+ oxidation state. The FT-XANES (Figure 4D) data suggest that the samples all exhibit the molecular states. We assumed that P₁G-Co²⁺ has been stabilized at a higher oxidation state at the open circuit condition, which made the Co^{2+/3+} redox less prominent. Since the redox of P₁G-Co²⁺ is typically a PCET process as inferred from the above Pourbaix result, the Co sites of P₁G-Co²⁺ could also interact with OH⁻ ions in the alkaline solution without external bias. This could change the oxidation states of Co sites through the coupled electron transfer. To verify such an assumption, P₁G-Co²⁺ and P₃G-Co²⁺ were titrated with KOH solution under the recording of UV/Vis measurements (Figure S20). The MLCT band of Co(acac)₂ showed a significant blue shift with the continuous titration of KOH solution, indicating that the electron transition from Co²⁺ ions to ligands requires higher excitation energy. This is attributed to the ligand exchange from acac⁻ to OH⁻ ions as previously reported.^[4b,c] Due to the π^* orbitals of acac⁻, the MLCT of Co(acac)₂ is relatively energetically favored, while OH⁻ ions

do not contain π^* orbitals to support MLCT, which explains the observed blue shift. In the case of P₁G-Co²⁺, a similar blue shift was observed, illustrating that the OH⁻ ions gradually attached to Co sites. In contrast, the MLCT of P₃G-Co²⁺ remained constant in the KOH titration. This is further verified by the corresponding XPS surveys (Figure S21). After immersing P₁G-Co²⁺ into the KOH solution, the strong Co 2p satellites disappeared, indicating the conversion from 2+ to 3+ oxidation state.^[18] Under the same conditions, the Co 2p satellites of P₃G-Co²⁺ well remained. These data fully support that Co sites of P₁G-Co²⁺ have been increased to the 3+ oxidation state through the OH⁻ ions coupling at the open circuit, and it changed the redox properties of P₁G-Co²⁺.

We next investigated the structures of P dopants of reduced graphene oxide to verify if they caused the tuned oxidation state of Co sites. As presented by XPS surveys (Figure 4E), the P 2p core levels of P₁G centered at 134.5 eV, which is assigned to highly oxidized PO(OH)₂ species.^[19] In contrast, the P 2p core levels of P₃G centered at 133.2 eV. This indicated the relatively low oxidized P

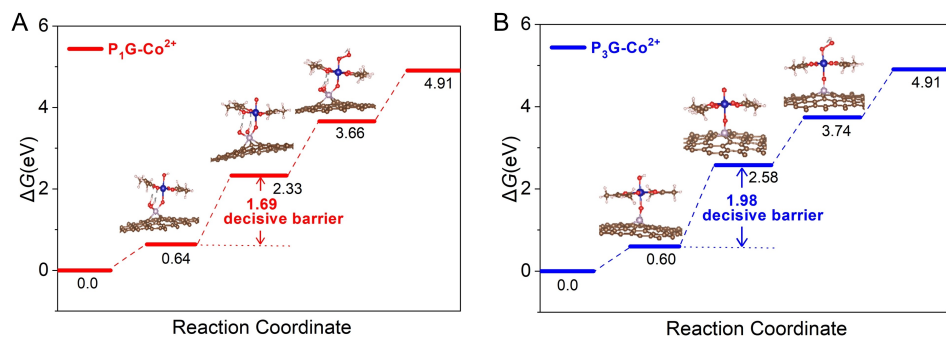


Figure 5. OER barriers on molecular Co sites. The OER free energy diagrams on simulated $P_1G\text{-Co}^{2+}$ (A) and $P_3G\text{-Co}^{2+}$ (B).

dopants assigning to PO species.^[19–20] The P 2p core levels of P_2G were deconvoluted to contain both PO(OH)_2 and PO species. In the solid-state ^{31}P nuclear magnetic resonance (NMR) spectra (Figure 4F), P_3G exhibited a wide signal at 13 ppm for low oxidized phosphorus species,^[21] while the main peak of P_1G shifted to a high field of 19.5 ppm, indicating the increased oxidized states of phosphorus species.^[22] P_2G contains both the features of phosphorus species of P_1G and P_3G . Correspondingly, we conducted the density functional theory calculations, and established the models of $P_1G\text{-Co}^{2+}$ and $P_3G\text{-Co}^{2+}$ based on the above XPS P 2p, ^{31}P NMR and FT EXAFS fitting analysis (Figure S22). The charge density difference of two configurations was compared (Figure 4G and 4H). For $P_1G\text{-Co}^{2+}$, charges flowed from the Co sites to the PO(OH)_2 ligands. While for $P_3G\text{-Co}^{2+}$, there were less charges transferring from the Co sites to the acac⁻ ligands, and the incorporated PO ligands did not exhibit clear charge exchange behaviors with the Co sites. In addition, the Bader charge calculations showed that upon the chemisorption of OH species, approximately 2.2e^- ($P_1G\text{-Co}^{2+}$) and 1.1e^- ($P_3G\text{-Co}^{2+}$) charges were transferred from the Co site to OH species, respectively. This is consistent with the above CV, UV/Vis and XPS analysis, and again it indicated that the coupling of OH^- ions drove the increased Co oxidation states of $P_1G\text{-Co}^{2+}$ through the linking of PO(OH)_2 species. Toward the electrocatalysis of OER, the decisive step on $P_1G\text{-Co}^{2+}$ and $P_3G\text{-Co}^{2+}$ are both the removal of one H atom from OH^* to generate an O^* in the surface adsorption state. This step is easier on $P_1G\text{-Co}^{2+}$ with an energy barrier of 1.69 eV, while the energy barrier increased to 1.98 eV on $P_3G\text{-Co}^{2+}$ (Figure 5).

Conclusion

In summary, P atoms doped reduced graphene oxide was synthesized by a common hydrothermal method, which served as a solid support of molecular Co sites toward synthesizing novel HMCs, and the oxidation properties of linked Co sites were tuned. The P dopants in reduced graphene oxide were regulated to achieve a highly oxidized PO(OH)_2 species. Through the linkage of PO(OH)_2 species, the molecular Co sites were spontaneously oxidized from 2+ to 3+ states in a KOH solution through OH^- ions

coupling at an open circuit condition due to the PCET nature of Co sites. The Co^{3+} sites were thus stabilized prior to the OER cycles, which greatly promoted the OER activity by affording a high TOF of 0.87 s^{-1} at an overpotential of 0.35 V. Our research provides a novel mechanism insight into Co based OER catalysis, and is beneficial for the rational design of high-performance HMCs.

Acknowledgements

The authors gratefully acknowledge the support from the National Natural Science Foundation of China (Grant No. 22002119), the National Natural Science Foundation of Jiangsu, China (Grant No. BK20200261) and the Programs of Science and Technology of Suzhou, China (Grant Nos. ZXL2021448, SYG202137). X.W. acknowledges the grants by the City University of Hong Kong (Grant Nos. 9020005, 9610663, 7020103), ITF - RTH - Global STEM Professorship (Grant No. 9446008), and Hong Kong Branch of National Precious Metals Material Engineering Research Center - ITC Fund.

Conflict of Interest

The authors declare no conflict of interest.

Data Availability Statement

The data that support the findings of this study are available from the corresponding author upon reasonable request.

Keywords: Transition metal ion redox · proton-coupled electron transfer · molecular electrocatalysis · oxygen evolution · alkaline water electrolysis

- [1] a) Z. Y. Yu, Y. Duan, X. Y. Feng, X. X. Yu, M. R. Gao, S. H. Yu, *Adv. Mater.* **2021**, *33*, 2007100; b) R. Abbasi, B. P. Setzler, S. S. Lin, J. H. Wang, Y. Zhao, H. Xu, B. Pivovar, B. Y. Tian, X. Chen, G. Wu, Y. S. Yan, *Adv. Mater.* **2019**, *31*, 1805876; c) I. Roger, M. A. Shipman, M. D. Symes, *Nat. Chem. Rev.* **2017**, *1*,

- 0003; d) M. G. Walter, E. L. Warren, J. R. McKone, S. W. Boettcher, Q. Mi, E. A. Santori, N. S. Lewis, *Chem. Rev.* **2010**, *110*, 6446; e) M. Chatenet, B. G. Pollet, D. R. Dekel, F. Dionigi, J. Deseure, P. Millet, R. D. Braatz, M. Z. Bazant, M. Eikerling, I. Staffell, P. Balcombe, Y. Shao-Horn, H. Schäfer, *Chem. Soc. Rev.* **2022**, *51*, 4583; f) T. Sun, Z. Tang, W. Zang, Z. Li, J. Li, Z. Li, L. Cao, J. S. Dominic Rodriguez, C. O. M. Mariano, H. Xu, P. Lyu, X. Hai, H. Lin, X. Sheng, J. Shi, Y. Zheng, Y.-R. Lu, Q. He, J. Chen, K. S. Novoselov, C.-H. Chuang, S. Xi, X. Luo, J. Lu, *Nat. Nanotechnol.* **2023**, *18*, 763; g) Z. Li, Z. Wang, S. Xi, X. Zhao, T. Sun, J. Li, W. Yu, H. Xu, T. S. Herng, X. Hai, P. Lyu, M. Zhao, S. J. Pennycook, J. Ding, H. Xiao, J. Lu, *ACS Nano* **2021**, *15*, 7105; h) X. Li, S. Mitchell, Y. Fang, J. Li, J. Perez-Ramirez, J. Lu, *Nat. Chem. Rev.* **2023**, *7*, 754; i) T. Sun, W. Zang, H. Yan, J. Li, Z. Zhang, Y. Bu, W. Chen, J. Wang, J. Lu, C. Su, *ACS Catal.* **2021**, *11*, 4498.
- [2] a) R. R. Rao, M. J. Kolb, N. B. Halck, A. F. Pedersen, A. Mehta, H. You, K. A. Stoerzinger, Z. Feng, H. A. Hansen, H. Zhou, L. Giordano, J. Rossmeisl, T. Vegge, I. Chorkendorff, I. E. L. Stephens, Y. Shao-Horn, *Energy Environ. Sci.* **2017**, *10*, 2626; b) Y. Lee, J. Suntivich, K. J. May, E. E. Perry, Y. Shao-Horn, *J. Phys. Chem. Lett.* **2012**, *3*, 399.
- [3] a) X. Peng, X. Jin, B. Gao, Z. Liu, P. K. Chu, *J. Catal.* **2021**, *398*, 54; b) M. Yu, E. Budiyanto, H. Tüysüz, *Angew. Chem. Int. Ed.* **2022**, *61*, e202103824.
- [4] a) M. Risch, F. Ringleb, M. Kohlhoff, P. Bogdanoff, P. Chernev, I. Zaharieva, H. Dau, *Energy Environ. Sci.* **2015**, *8*, 661; b) J. Wang, X. Ge, Z. Liu, L. Thia, Y. Yan, W. Xiao, X. Wang, *J. Am. Chem. Soc.* **2017**, *139*, 1878; c) H. Yang, F. Li, S. Zhan, Y. Liu, W. Li, Q. Meng, A. Kravchenko, T. Liu, Y. Yang, Y. Fang, L. Wang, J. Guan, I. Furó, M. S. G. Ahlquist, L. Sun, *Nat. Catal.* **2022**, *5*, 414; d) Q. B. Wu, J. W. Liang, M. J. Xiao, C. Long, L. Li, Z. H. Zeng, A. Mavric, X. Zheng, J. Zhu, H. W. Liang, H. F. Liu, M. Valant, W. Wang, Z. X. Lv, J. Li, C. H. Cui, *Nat. Commun.* **2023**, *14*, 997.
- [5] B. Wang, Y.-M. Lee, W.-Y. Tcho, S. Tussupbayev, S.-T. Kim, Y. Kim, M. S. Seo, K.-B. Cho, Y. Dede, B. C. Keegan, T. Ogura, S. H. Kim, T. Ohta, M.-H. Baik, K. Ray, J. Shearer, W. Nam, *Nat. Commun.* **2017**, *8*, 14839.
- [6] M. N. Jackson, C. J. Kaminsky, S. Oh, J. F. Melville, Y. Surendranath, *J. Am. Chem. Soc.* **2019**, *141*, 14160.
- [7] a) J. Wang, S. Dou, X. Wang, *Sci. Adv.* **2021**, *7*, eabf3989; b) Y. Wu, Y. Liang, H. Wang, *Acc. Chem. Res.* **2021**, *54*, 3149; c) D. Grammatico, A. J. Bagnall, L. Riccardi, M. Fontecave, B.-L. Su, L. Billon, *Angew. Chem. Int. Ed.* **2022**, *61*, e202206399; d) X. J. Cui, W. Li, P. Ryabchuk, K. Junge, M. Beller, *Nat. Catal.* **2019**, *2*, 277.
- [8] a) A. K. Vannucci, L. Alibabaei, M. D. Losego, J. J. Conception, B. Kalanyan, G. N. Parsons, T. J. Meyer, *Proc. Nat. Acad.* **2003**, *100*, 20918; b) Y. Wang, F. Li, X. Zhou, F. Yu, J. Du, L. Bai, L. Sun, *Angew. Chem. Int. Ed.* **2017**, *56*, 6911; c) T. Cuk, *ACS Cent. Sci.* **2018**, *4*, 1084; d) M. N. Jackson, Y. Surendranath, *Acc. Chem. Res.* **2019**, *52*, 3432.
- [9] M. A. Patel, F. Luo, M. R. Khoshi, E. Rabie, Q. Zhang, C. R. Flach, R. Mendelsohn, E. Garfunkel, M. Szostak, H. He, *ACS Nano* **2016**, *10*, 2305.
- [10] X. D. Long, Z. L. Li, G. Gao, P. Sun, J. Wang, B. S. Zhang, J. Zhong, Z. Jiang, F. W. Li, *Nat. Commun.* **2020**, *11*, 4074.
- [11] S. Yamauchi, M. Tanabe, K. Takahashi, S. Islam, H. Matsuoka, Y. Ohba, *Appl. Magn. Reson.* **2010**, *37*, 317.
- [12] J. Wang, L. Gan, W. Zhang, Y. Peng, H. Yu, Q. Yan, X. Xia, X. Wang, *Sci. Adv.* **2018**, *4*, eaap7970.
- [13] Y. Xue, S. J. Traina, *Environ. Sci. Technol.* **1996**, *30*, 1975.
- [14] a) A. Bergmann, T. E. Jones, E. Martinez Moreno, D. Teschner, P. Chernev, M. Gleich, T. Reier, H. Dau, P. Strasser, *Nat. Catal.* **2018**, *1*, 711; b) W. Zheng, M. Liu, L. Y. S. Lee, *ACS Catal.* **2019**, *10*, 81.
- [15] Y. He, F. Guo, K. R. Yang, J. A. Heinlein, S. M. Bamonte, J. J. Fee, S. Hu, S. L. Suib, G. L. Haller, V. S. Batista, L. D. Pfefferle, *J. Am. Chem. Soc.* **2020**, *142*, 17119.
- [16] M. Li, X. Wang, K. Liu, H. Sun, D. Sun, K. Huang, Y. Tang, W. Xing, H. Li, G. Fu, *Adv. Mater.* **2023**, *35*, 2302462.
- [17] K. Du, L. Zhang, J. Shan, J. Guo, J. Mao, C.-C. Yang, C.-H. Wang, Z. Hu, T. Ling, *Nat. Commun.* **2022**, *13*, 5448.
- [18] a) E. S. Andreiadis, P.-A. Jacques, P. D. Tran, A. Leyris, M. Chavarot-Kerlidou, B. Jousselme, M. Matheron, J. Pécaut, S. Palacin, M. Fontecave, V. Artero, *Nat. Chem.* **2013**, *5*, 48; b) H. Chen, L. J. Falling, H. Kersell, G. Yan, X. Zhao, J. Oliver-Meseguer, M. Jaugstetter, S. Nemsak, A. Hunt, I. Waluyo, H. Ogasawara, A. T. Bell, P. Sautet, M. Salmeron, *Nat. Commun.* **2023**, *14*, 6889.
- [19] G. Hasegawa, T. Deguchi, K. Kanamori, Y. Kobayashi, H. Kageyama, T. Abe, K. Nakanishi, *Chem. Mater.* **2015**, *27*, 4703.
- [20] Z. Bi, L. Huo, Q. Kong, F. Li, J. Chen, A. Ahmad, X. Wei, L. Xie, C.-M. Chen, *ACS Appl. Mater. Interfaces* **2019**, *11*, 11421.
- [21] A. Seitkhan, M. Neophytou, M. Kirkus, E. Abou-Hamad, M. N. Hedhili, E. Yengel, Y. Firdaus, H. Faber, Y. Lin, L. Tsetseris, I. McCulloch, T. D. Anthopoulos, *Adv. Funct. Mater.* **2019**, *29*, 1905810.
- [22] a) M. Köllo, M. Kudrjašova, M. Kulp, R. Aav, *Anal. Methods* **2013**, *5*, 4005; b) B. J. Cade-Menun, *Talanta* **2005**, *66*, 359.

Manuscript received: August 24, 2024

Accepted manuscript online: October 10, 2024

Version of record online: November 7, 2024